



CASE REPORT

CNS Embryonal Tumour with Desmoplastic Reaction Treated with Ultra-NPT Bionanocatalysts

Tessy Lopez-Goerne^{1,2*}, Francisco J Padilla-Godínez^{1,3}, Daniel Álvarez-Amador¹, Antonela Gonzalez-Bondani¹, Rafael Valiente¹, Fernando Chico Ponce de Leon³, Vicente Gonzalez-Carranza⁴ José Omar Navarro-Fernández⁵ and Abel Santamaria¹

¹Department of Health Care, Autonomous Metropolitan University-Xochimilco, Mexico

²Department of Chemical and Biomolecular Engineering, Tulane University, USA

³Department of Mathematics and Physics, Western Institute of Technology and Higher Education, Mexico

⁴Department of Neurology and Neurosurgery, Children's Hospital of Mexico "Federico Gomez", Mexico

⁵Department of Head and Neck, National Institute of Cancerology, Mexico

***Corresponding author:** Tessy López-Goerne, Laboratory of Nanotechnology and Nanomedicine, Department of Health Care, Autonomous Metropolitan University-Xochimilco, Mexico City 04960, Mexico



Abstract

Central nervous system (CNS) embryonal tumors, lacking a distinct molecular signature and categorized as "Not Otherwise Specified (NOS)", are WHO grade IV neoplasms with significant genetic diversity. They typically exhibit immature cell sheets with round, oval, or angulated nuclei, often located supratentorially and characterized by a desmoplastic reaction. Diagnosis relies on MRI and molecular analysis, with traditional management involving surgery, radiotherapy, and chemotherapy. However, recurrence rates remain high, with reported 3-year survival rates of 57%-73%. Recent research explores targeted therapies such as bionanocatalysts, showing promise in eradicating tumors with minimal side effects, as demonstrated in the present case report.

Keywords

Brain tumor, Bionanocatalyst, Ultra-NPt, Central nervous system, Embryonal tumor NOS

classified as WHO grade IV neoplasms, exhibit significant genetic heterogeneity, featuring densely packed sheets of immature cells with a high nucleus-to-cytoplasm ratio and nuclei typically round, oval, or angulated [2]. Predominantly supratentorial in location, these tumors are usually well-defined and solid, though they may exhibit cystic areas, hemorrhage, and necrosis. Additionally, they often incite a desmoplastic reaction, marked by the formation of fibrous tissue around the tumor as an immune response to malignancy [3,4].

Diagnosis heavily relies on imaging modalities, primarily magnetic resonance imaging (MRI), following the identification of neurological signs and symptoms [5]. Subsequent molecular analysis is crucial for accurate diagnosis and subsequent treatment planning. Diagnostic criteria encompass the presence of a CNS embryonal tumor with molecular analysis failing to place it within a more specific subtype [6].

Traditional management of these neoplasms involves total surgical resection followed by radiotherapy directed to the neuroaxis, with adjuvant chemotherapy potentially enhancing patient survival. However, despite multimodal therapy, prognosis remains grim, with recurrence common, particularly in the early post-

Introduction

Central nervous system (CNS) embryonal tumors constitute a diverse category characterized by embryonal histology and immunophenotype, yet lacking a distinctive molecular signature, thus categorized as "Not Otherwise Specified (NOS)" [1]. These tumors,



Citation: López-Goerne T, Padilla-Godínez FJ, Álvarez-Amador D, Gonzalez-Bondani A, Valiente R, et al. (2024) CNS Embryonal Tumour with Desmoplastic Reaction Treated with Ultra-NPT Bionanocatalysts. Neurosurg Cases Rev 7:161. doi.org/10.23937/2643-4474/1710161

Accepted: July 04, 2024; **Published:** July 06, 2024

Copyright: © 2024 López-Goerne T, et al. This is an open-access article distributed under the terms of the Creative Commons Attribution License, which permits unrestricted use, distribution, and reproduction in any medium, provided the original author and source are credited.

treatment period, yielding reported 3-year survival rates ranging from 57% to 73% [7].

Recent research endeavors have aimed at developing targeted technologies for cancer cell elimination while sparing normal tissues [8-10]. Notably, bionanocatalysts have emerged as a promising avenue, possessing the capability for selective bond-breakage in mitochondrial and nuclear DNA [11]. The current case report highlights the successful application of ultra-small bionanocatalysts in treating a patient with CNS NOS embryonal tumor, resulting in tumor eradication without discernible side effects.

Materials and Methods

The ultra-NPt bionanocatalysts were synthesized using established methods [12] with modifications to various parameters, including pH of gelation, type of alkoxide, solvent type, stirring method, reactor setup, concentration of reagents, and temperature control. Surface coating of ultra-NPt particles (NPt \leq 5 nm) is crucial for reducing additive-induced toxicity and enhancing biocompatibility. This coating involves dispersing platinum on functionalized titania surfaces with zwitterionic ligands via weak bonds. The coating's universality enables versatile surface functionalization, offering significant potential for these bionanocatalysts in cancer treatment.

Electron microscopy analysis

For analysis, electron microscopy (TEM) was utilized to determine particle size, using a Zeiss EM910 electron microscope operated at 100 kV with a 0.4 nm resolution side entry goniometer and CCD Mega Vision III image processor.

X-ray diffraction studies

X-ray diffraction studies employed a Siemens D500 diffractometer with a copper or molybdenum anode tube, generating radial distribution functions for high angular parameter values using the Radiale program.

Histopathological analysis

Histopathological analysis, crucial for intraoperative assessment, relied on the Hematoxylin-Eosin (H&E) staining technique. H&E staining, employing hematoxylin for nuclear structures and eosin for cytoplasmic components, provided visualization under a light microscope. Standard H&E staining procedures were conducted [13].

Clinical Case

Clinical history

The patient presented with symptoms of headaches and seizures, without significant prior medical history. A cranial computed tomography (CT) scan revealed a sizable intracranial lesion, prompting surgical intervention for its removal in July 2018.

Subsequent histopathological analysis confirmed a grade 4 Embryonal Tumor with Desmoplastic Reaction NOS, according to the CNS5 Classification outlined in the WHO 2021 guidelines. Following resection, the patient underwent radiotherapy and chemotherapy regimen involving carboplatin and cyclophosphamide. Neurological deficits, including decreased strength on the left side and chemotherapy-induced side effects, were observed postoperatively. However, over the ensuing weeks, significant improvement was noted, leading to almost complete resolution of neurological deficits. The patient was prescribed levetiracetam for one year as a prophylactic measure against seizures.

The patient underwent regular follow-up assessments, including laboratory tests and imaging studies every 4-6 months, revealing no evidence of tumor recurrence. Throughout the postoperative period, the patient remained asymptomatic. To further monitor her condition, lumbar puncture was performed to exclude neoplastic cell presence, alongside a PET scan, revealing hypometabolism at the site of the previous tumor resection in the right parietal region. Subsequent cytochemical and cytopathological analyses from a second lumbar puncture yielded normal results, indicating the absence of malignant cells. The patient received levetiracetam orally until symptom-free, gradually discontinuing the medication.

Control assessments consistently showed no tumor recurrence. Radiotherapy, administered from September to October 2018 with 60 Gy in 30 fractions, and chemotherapy with temozolomide for six months, constituted the initial postoperative treatment regimen.

During follow-up MRI evaluations, a new lesion, identified as a meningioma measuring 2 cm in diameter in the right frontoparietal region, was detected in August 2020. Subsequent surgical intervention utilizing neuronavigation ensured complete macroscopic resection of the tumor mass, leading to total neurological improvement. Additional radiotherapy, with another dose of 60 Gy in 30 fractions, was administered from November 2020 to January 2021. Chemotherapy was modified to Lomustine, Vincristine, and Procarbazine.

In May 2023, MRI revealed tumor recurrence involving the surgical bed, posterior insula, superior temporal gyrus, and supramarginal gyrus, measuring 4 × 4 × 4 in size, as depicted in [Figure 1](#) and [Figure 2](#).

The decision was made to proceed with a third surgery. During this procedure, following the removal of the recurrent tumor, the entirety of the surgical site, encompassing the posterior region of the insula, superior temporal gyrus, and supramarginal gyrus, was treated with the application of ultra-NPt bionanocatalysts ([Figure 3](#)).

Post-Surgery MRI analyses

The MRI conducted in May 2023, prior to nanoparticle

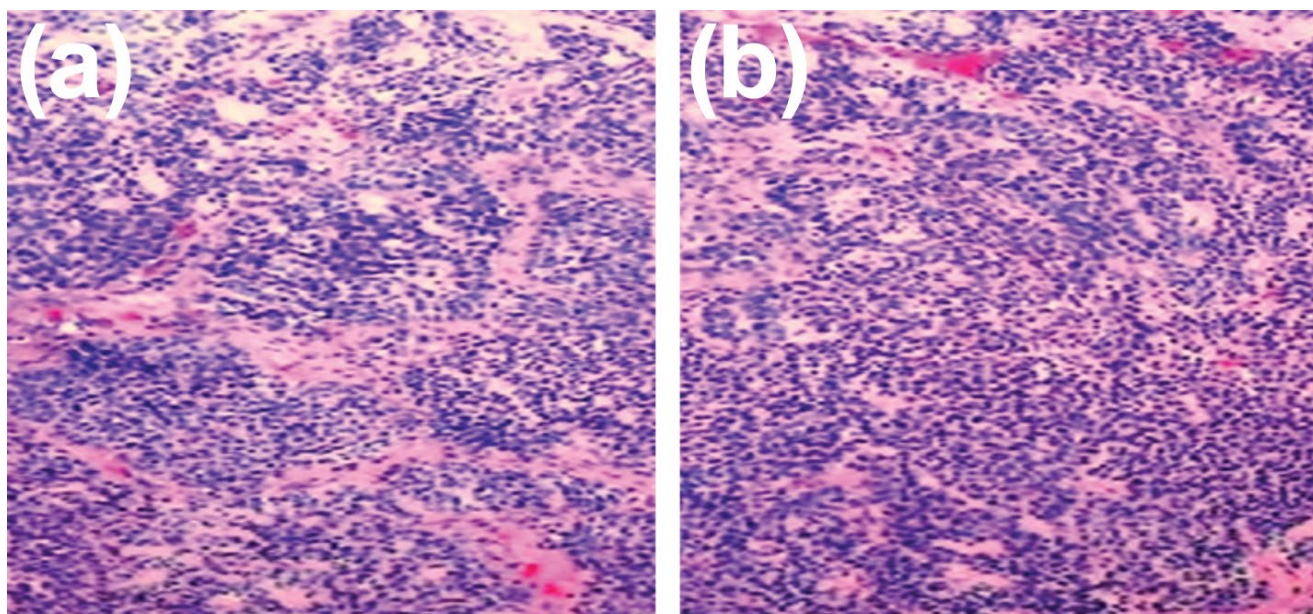


Figure 1: Histopathological examination of the resected tumor. Microscopic analysis reveals the presence of immature cells characterized by a high nucleus-to-cytoplasm ratio, along with round, oval, or angulated hyperchromatic nuclei. These features are indicative of the tumor's embryonal nature. Micrographs were captured at 20X magnification for detailed examination.

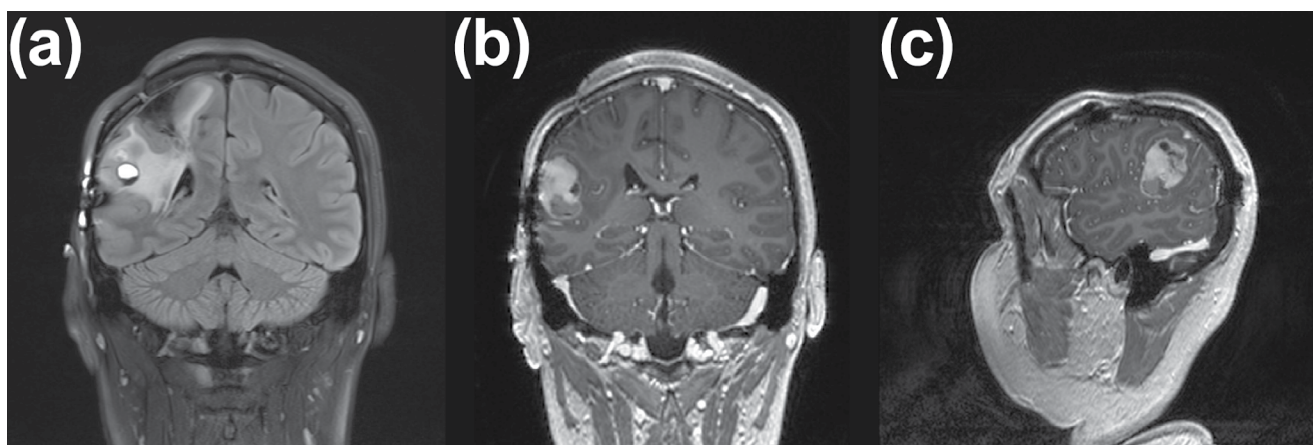


Figure 2: MRI Findings, May 2023. The MRI images depict post-surgical alterations in the right parietal region, along with gliosis in the right superior parietal lobule. Notably, a mixed intra-axial lesion is evident, characterized by solid and liquid components with a level effect, measuring up to 2.5 × 3 cm in the postcentral gyrus and supramarginal gyrus. This lesion exhibits heterogeneous densities in T2/FLAIR sequences, restricted diffusion in DWI, and low values of ADC, alongside irregular contrast medium uptake and perilesional cerebral edema in the occipital horn and right atrium. Importantly, there is no displacement of cerebral structures or midline shift observed.

placement (Figure 4A, Figure 4B and Figure 4C), revealed a hyperintense image in the correct surgical bed, involving the posterior region of the insula, superior temporal gyrus, and supramarginal gyrus, evident in the T2 and Flair pulse sequences. This area appeared hypointense in T1, with focal areas of hyperintensity suggestive of methemoglobin, alongside haemosiderin deposits both internally and peripherally, as well as images displaying a liquid-liquid level. The described image measured 2.1 × 2.2 cm in the axial plane, 2 × 2.2 cm in the coronal plane, and 2.3 × 2.3 cm in the sagittal plane, showing intense enhancement with contrast medium. Additionally, peripheral hyperintensity was

observed in the T2 and Flair pulse sequences between the surgical bed and the lateral ventricle wall, atrium, and corresponding superior temporal gyrus. Increased thickness of cerebral gyri, with mass effect on those corresponding to the dorsal region of the insula, was noted, along with obliteration of adjacent subarachnoid spaces. Haemosiderin deposits were also identified in the posterior frontoparietal region. Notably, increased mean transit time and cerebral blood volume were observed at the neurosurgical site during the perfusion phase.

Following the placement of ultra-nanoparticles, a control MRI was performed in September 2023 (Figure

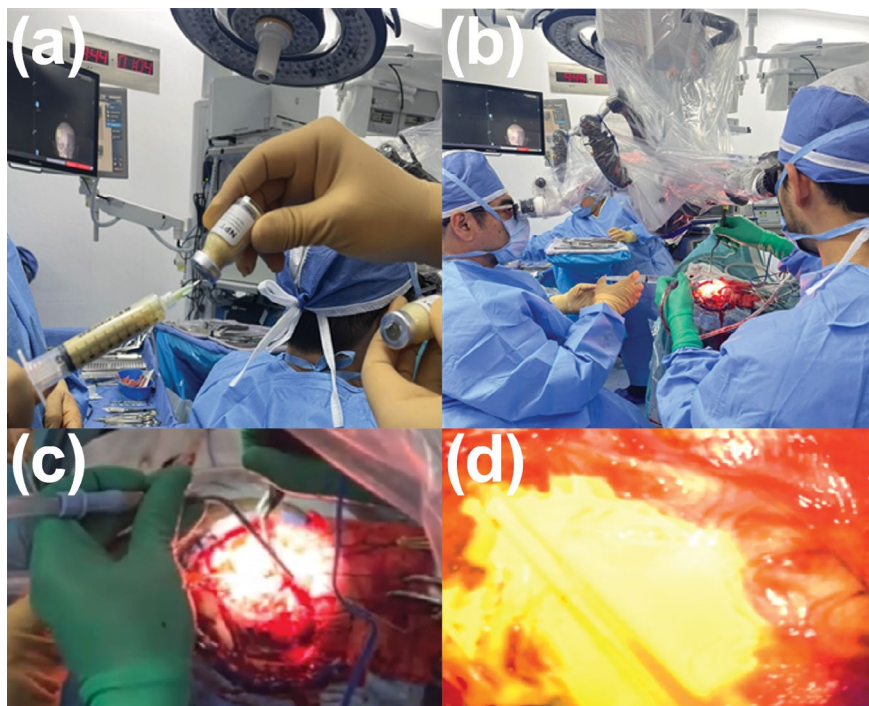


Figure 3: Surgical Deposition of Ultra-NPt Bionanocatalysts in the Tumor Bed after Resection. a) Preparation of ultra-npt Bionanocatalysts; b) Administration of Ultra-NPt Bionanocatalysts; c) Tumor bed exposed for incorporation; d) Tumor bed covered with Ultra-NPt bionanocatalysts.

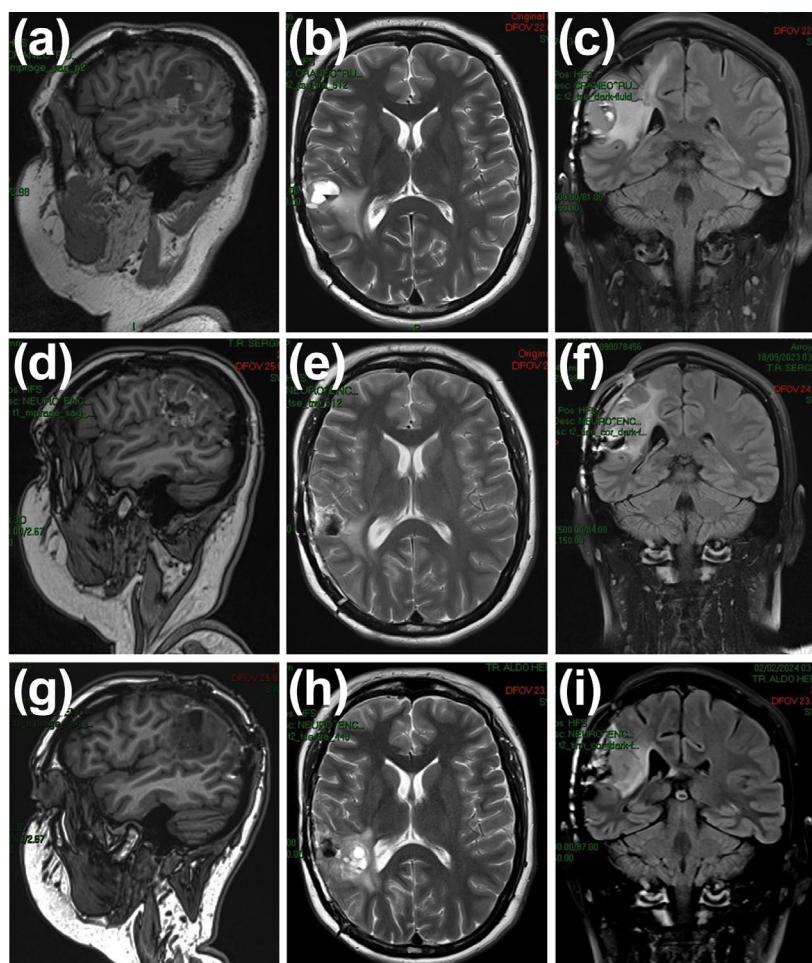


Figure 4: MRI of the cerebellum. May 2023. a) Sagittal section in T1 sequence; b) Axial section in T2 sequence; c) Coronal section in T2 FLAIR sequence. September 2024; d) Sagittal section in T1 sequence; e) Axial section in T2 sequence; f) Coronal section in T2 FLAIR sequence. February 2024; g) Sagittal section in T1 sequence; h) Axial section in T2 sequence; i) Coronal section in T2 FLAIR sequence.

4D, Figure 4E and Figure 4F), revealing surgical changes due to tumor resection at the right frontotemporal level. A hematoma of the surgical bed with axial axes measuring 2.9 cm × 2.2 cm was observed in the axial plane, displaying heterogeneously high signal intensity in T2-weighted sequences, with a hyperintense halo in pre-contrast T1 sequences and discrete peripheral enhancement post-contrast medium administration. Perilesional edema persisted, involving the subcortical and deep white matter of the right precentral gyrus, semiovale center, and ipsilateral superior temporal gyrus, albeit decreased compared to the previous study. Increased signal was noted within the ventricles and extra-axial space in the subarachnoid space between the sulci and fissures of the right parietal lobe adjacent to the surgical site, suggesting the presence of ultra-nanoparticles. Additionally, a laminar subdural collection measuring 5 mm thick was identified adjacent to the craniotomy site. Consequently, the medical committee decided to infiltrate the bionanocatalyst (ultra-NPt) given the recurrent nature of the tumor, with the expectation of complete tumor disappearance.

Notably, a simple and contrasted skull MRI of September 2023 displayed postoperative changes in

the right postcentral and supramarginal gyrus, with hematic debris in the surgical bed expected for the postoperative period, along with perilesional edema assessed in T2/FLAIR sequences. Minimal diffusion restriction and high ADC values were observed in the surgical site. Heterogeneous, linear, and diffuse uptake was evident in the surgical bed on T1+Gad images, as expected for the postoperative period. Multivoxel MRS revealed a choline peak and decreased NAA (Figure 5).

In February 2024, another control MRI was conducted, revealing discrete dilatation of the lateral ventricle and right atrium due to secondary traction (Figure 4G, Figure 4H and Figure 4I). The surgical bed exhibited approximate dimensions in the sagittal plane of 43 × 35 mm (previously 37 × 27 mm), coronal plane 42 × 31 mm (previously 40 × 17 mm), and axial 34 × 34 mm (previously 25 × 27 mm). Its signal intensity appeared heterogeneous, attributed to multiple cystic areas of varying dimensions surrounded by corticocortical hyperintensity indicating edema. This edema extended to the superior temporal gyrus, periventricular region, and dorsal aspect of the insula, involving the semioval center, pre- and postcentral gyrus, and the lateral margin of the corpus callosum. Notably, the cerebral

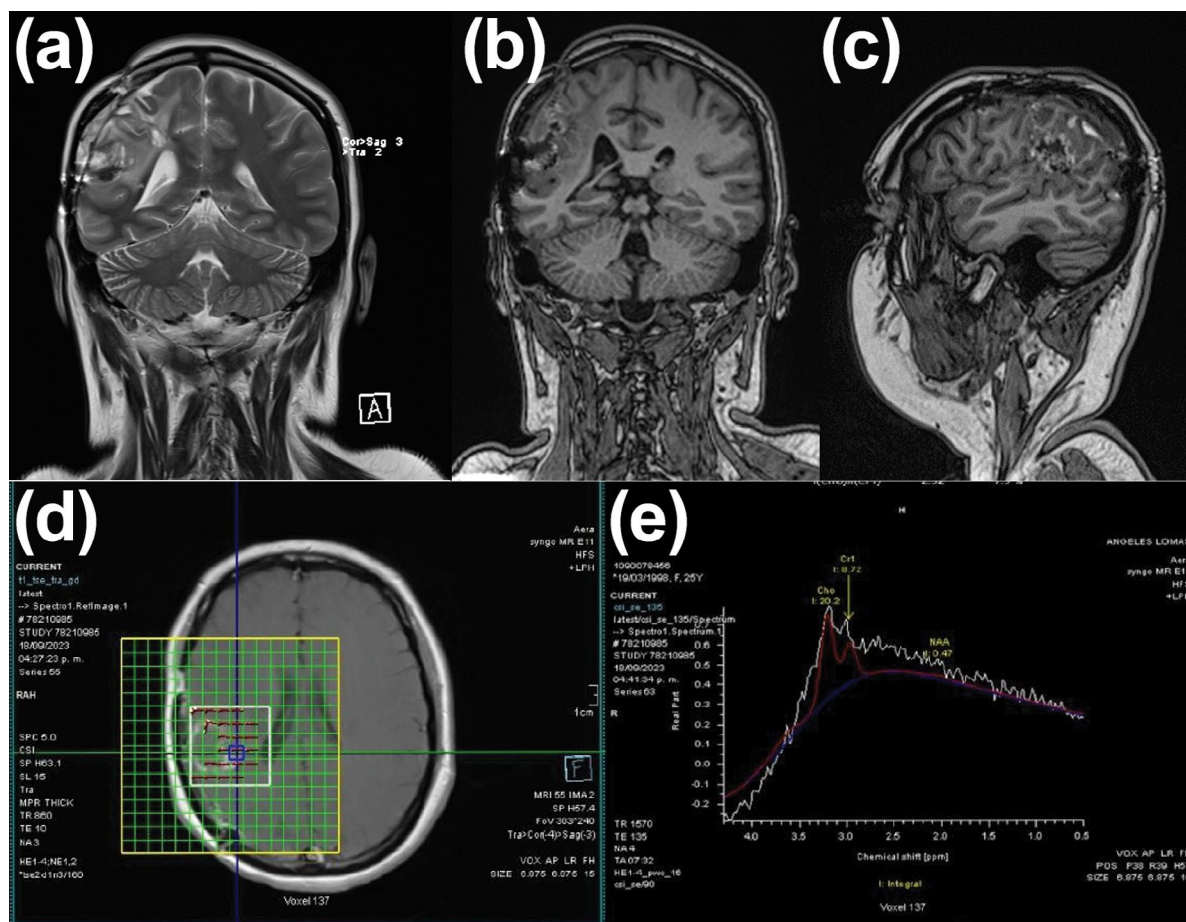


Figure 5: MRI of September 2023. The MRI depicts postoperative changes in the right postcentral and supramarginal gyrus, featuring hematic debris within the surgical bed, consistent with the expected findings for the postoperative period. Perilesional edema is observed in T2/FLAIR sequences. Notably, minimal diffusion restriction and high ADC values are noted in the surgical site. Furthermore, heterogeneous, linear, and diffuse uptake is evident in the surgical bed on T1+Gad images, as anticipated for the postoperative phase. Multivoxel MRS analysis reveals a choline peak and decreased NAA levels.

gyri corresponding to the third and fourth frontal gyri and the parietal lobe exhibited increased volume, with local subarachnoid spaces obliterated. Signal intensity restriction areas were observed within and medial to the surgical site, alongside identified haemosiderin deposits.

Compared to previous MRI scans, the peripheral edema around the right ventricular atrium, lateral ventricle, and parietal parenchyma was more pronounced, accompanied by evidence of remodeling and compression of these structures. Evaluation of the spinal cord revealed no changes in intensity (Figure 6), with the spinal canal and axial skeleton (vertebrae) exhibiting no alterations. Furthermore, the pelvic cavity showed no abnormalities, and no abnormal contrast medium accumulations were observed.

Discussion

The diagnosis and treatment of cancer hold immense significance due to the pervasive nature of the disease. Despite treatments like chemotherapy, surgery, and radiotherapy, tumors may regenerate over time [14]. Nanotechnology, with its rapid advancements, offers significant potential to revolutionize healthcare and challenge existing paradigms. Designing devices with unique therapeutic properties is crucial, as their small size enables deep infiltration into tumor cells with high specificity [15].

We developed (ultra-NPt) nanoparticles, characterized them, and tested their efficacy in various brain tumors [11,16,17]. These particles exhibited

substantial cytotoxic effects, leading to tumor size reduction. Brain cancer, especially in children, presents one of the most challenging prognoses [18]. Additionally, many patients present with widespread disease at diagnosis, rendering them incurable by surgical resection alone.

The infiltration of ultra-NPt bionanocatalyst particles serves as an adjuvant technology to inhibit tumor regrowth. Their promising application in brain cancer nanotherapy hinges on their ability to penetrate tumor cells selectively, sparing healthy ones [19]. Studies have shown cellular uptake of nanoparticles smaller than 5 nm, with various surface headgroups, facilitating efficient endocytosis [11]. Smaller particles exhibit enhanced cellular penetration and can even access the nucleus, influencing their excretion efficiency.

Ultra-NPt nanoparticles, possessing Pt (II) and Pt (IV) oxidation states along with Ti (III) and Ti (IV), pose a challenge in their synthesis [20]. However, their entry into cancer cells via endocytosis initiates a cascade of events within mitochondria. Vacuoles containing numerous bionanocatalytic particles target mitochondria, where they disrupt mitochondrial DNA bonds, generating reactive oxygen species (ROS) and triggering apoptosis. This process involves breaking C-C, C-N, and C-O bonds of mitochondrial DNA, ultimately leading to the formation of CO₂, H₂O, N₂, and free phosphates [11]. These actions are facilitated by the ultra-nanoparticulate and crystalline structure of ultra-NPt, as depicted in Figure 7.

Additionally, the introduction of transition metal

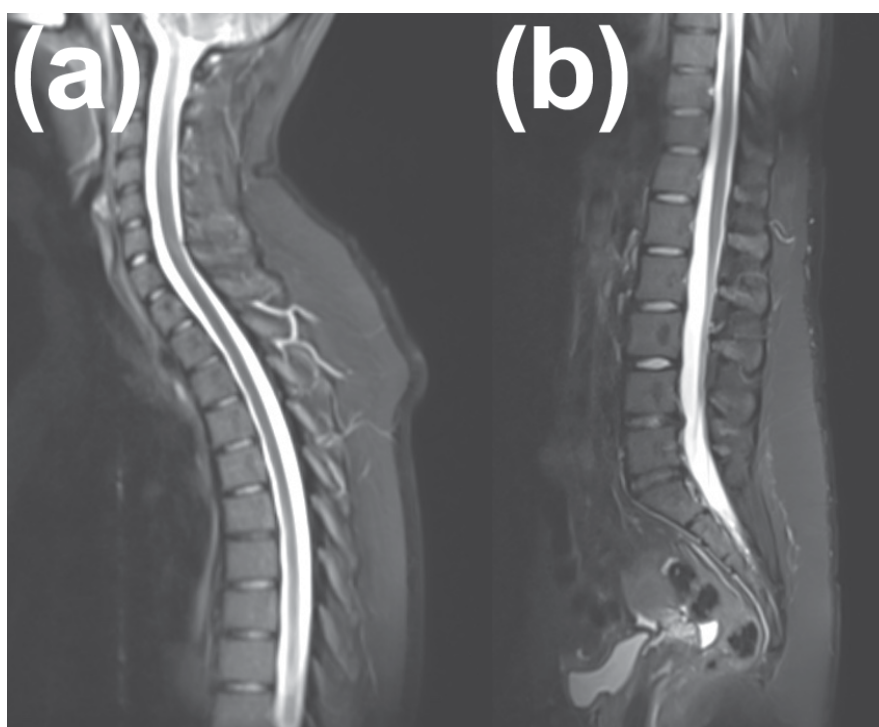


Figure 6: MRI of the Spinal Axis, February 2024. The MRI depicts a spinal cord of normal caliber and trajectory, without changes in intensity. Furthermore, the spinal canal and axial skeleton (vertebrae) exhibit no alterations. No abnormalities are noted in the pelvic cavity, and there are no abnormal accumulations of contrast medium observed.

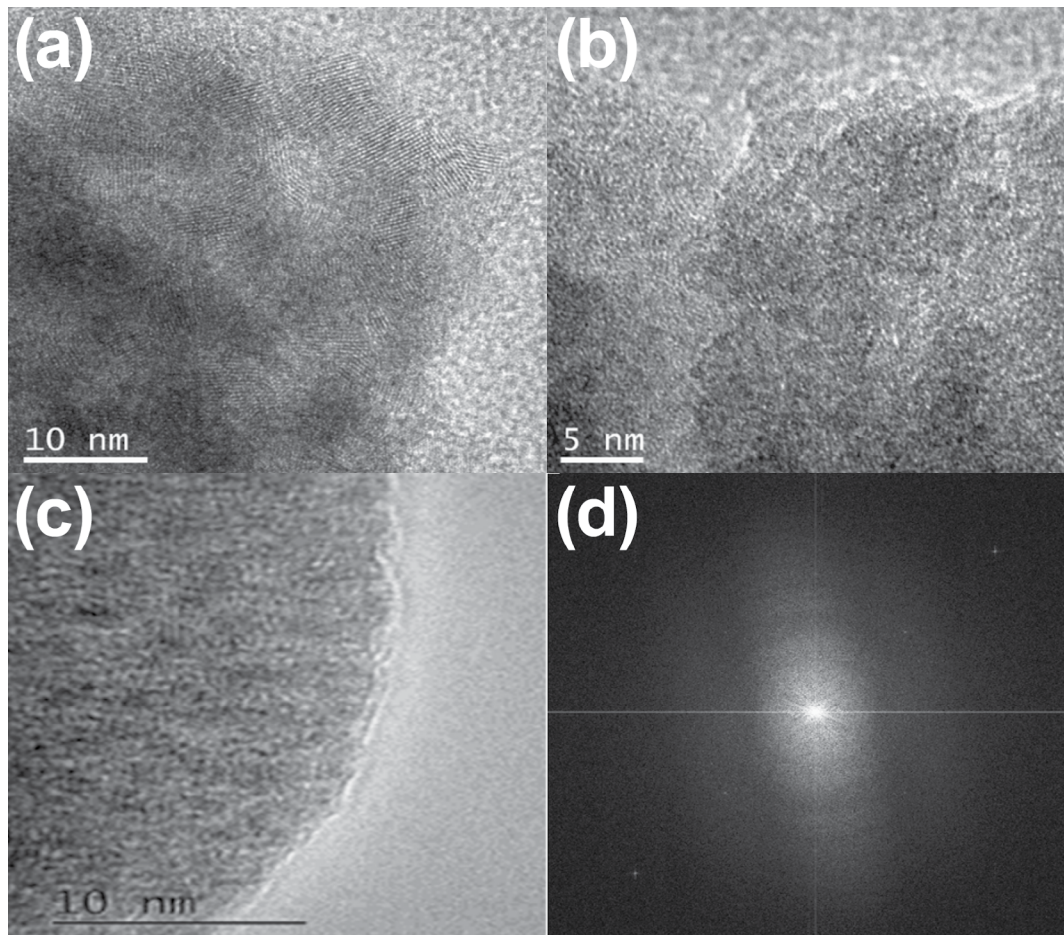


Figure 7: Transmission Electron Microscopy of Ultra-NPt Bionanocatalyst. The transmission electron microscopy image reveals ultra-nanoparticles smaller than 4.5 nm with remarkably high crystallinity. It is evident that platinum replicates the pure anatase lattice, as demonstrated by the electron diffraction pattern. This analysis was conducted at UAM Iztapalapa.

ions during synthesis typically influences the phase transformation behavior and structure of anatase [20]. Figure 8 displays diffractograms of the samples. All platinum/titania samples exhibited a single peak at 27.44 (2θ) corresponding to the anatase (1 0 1) phase. Notably, only anatase peaks were observed in ultra-NPt supported on functionalized TiO₂ samples. The nanostructured titania reference also displayed an anatase pattern.

Conclusions

In this study, a CNS NOS Embryonal Tumour with Desmoplastic Reaction was successfully treated using Ultra-NPt bionanocatalysts, showcasing their ability to selectively eliminate tumors while minimizing the secondary effects commonly associated with nanostructure use. This underscores their remarkable selectivity towards cancerous tissues while sparing healthy cells. This case report forms part of a broader project aimed at evaluating the effectiveness of oncological bionanocatalysts in treating brain neoplasms. The MRI analyses conducted to monitor the patient's progress provided crucial insights into the case's evolution. However, further studies are warranted to enhance our understanding of bionanocatalyst utilization in oncological treatments.

Ethics and Consent

The authors assert that all aspects of the investigation concerning human subjects in this study were conducted with the proper ethical clearance from pertinent authorities, and these approvals are duly recognized within the manuscript. The research adhered to the standards outlined by the National Institutes of Health and received explicit approval from the Ethics Committee of the Children's Hospital of Mexico under Protocol Number HIM 2017-072 entitled "Estudio del Efecto Antineoplásico del Nanomaterial Organoplatino al 1% Soportado en Titania Funcionalizada (NPt-Ped) en Niños con Tumores de Sistema Nervioso Central con Pronóstico Reservado en el Hospital Infantil de México 'Federico Gómez' y la Universidad Autónoma Metropolitana".

Supporting Information

All relevant information is included in the article.

Author Contribution

All authors contributed equally. All authors have given approval to the final version of the manuscript.

Acknowledgement and Funding

No acknowledgement nor funding to be declared.

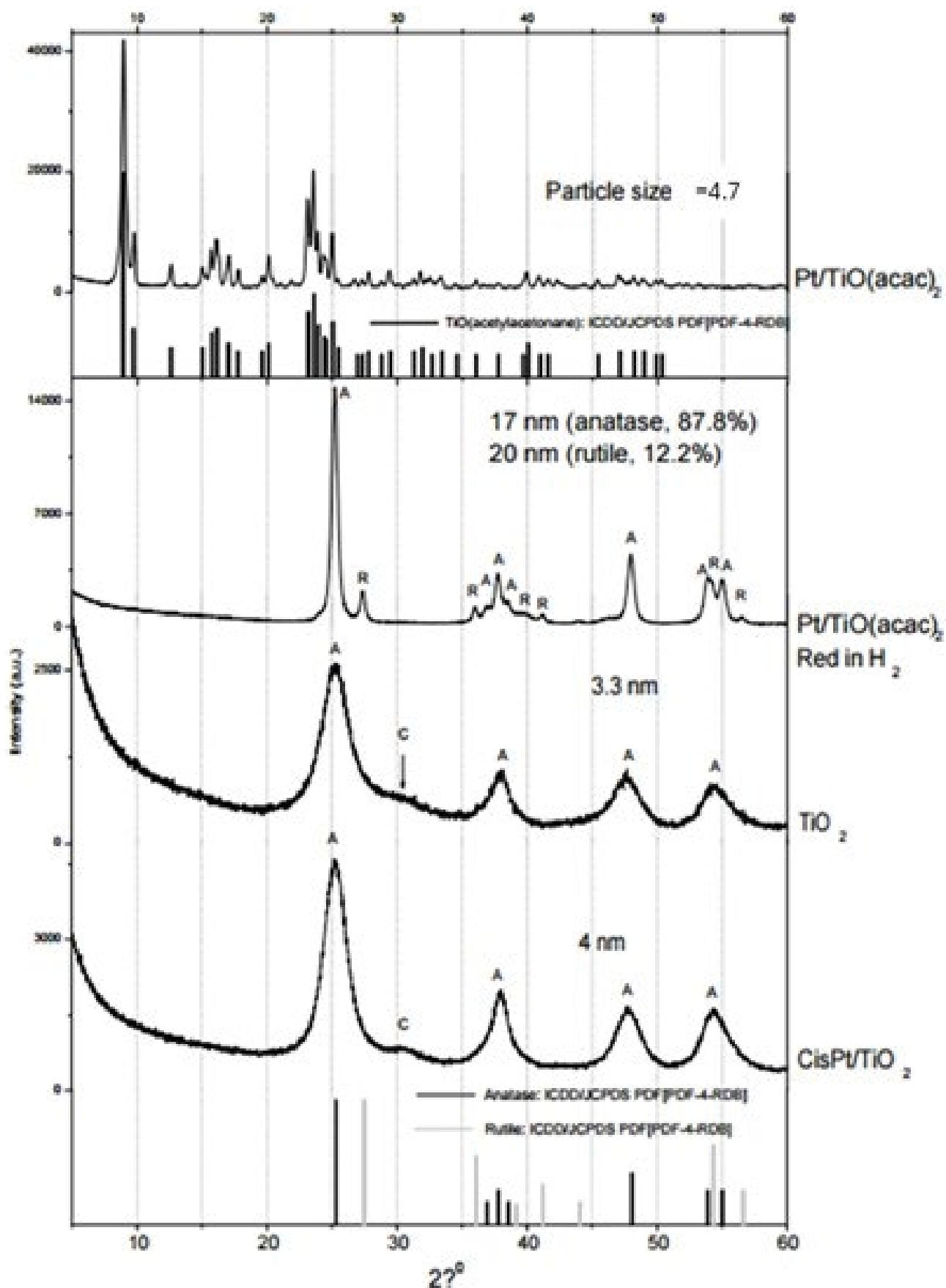


Figure 8: X-ray Diffraction (XRD) Analysis: i) Sol-gel CisPt/TiO₂ Nanoparticles (Reference): Particle size of 4 nm; ii) Sol-gel Titania (Reference): Particle size of 3.7 nm; iii) Organometallic Platinum Supported on Sol-gel Titania, Treated in H₂ for 4 Hours: This sample exhibits a mixture of traces of anatase and rutile phases, with larger particle sizes; iv) Organometallic Platinum Supported on Sol-gel Titania, Exclusive to Anatase Nanocrystals: Particle size approximately 4.7 nm.

References

1. Blessing MM, Alexandrescu S (2020) Embryonal tumors of the central nervous system. *Surg Pathol Clin* 13: 235-247.
2. Louis DN, Perry A, Wesseling P, Brat DJ, Cree IA, et al. (2021) The 2021 WHO classification of tumors of the central nervous system: A summary. *Neuro Oncol* 23: 1231-1251.
3. DeClerck YA (2012) Desmoplasia: A Response or a Niche? *Cancer Discov* 2: 772-774.
4. Abbas O, Mahalingam M (2011) Desmoplasia: Not always a bad thing. *Histopathology* 58: 643-659.
5. Patay Z (2022) Imaging embryonal tumors of the central nervous system. *Advances in Clinical Radiology* 4: 215-229.
6. Santosh V, Rao S, Dasgupta A, Gupta T (2021) Diagnosis and management of central nervous system embryonal tumors in the molecular era A contemporary review. *International Journal of Neuro-Oncology* 4: S190-S205.
7. Kram D, Henderson J, Baig M, Chakraborty D, Gardner MA, et al. (2018) Embryonal tumors of the central nervous system in children: The era of targeted therapeutics. *Bioengineering* 5: 78.
8. Rasool M, Malik A, Waquar S, Arooj M, Zahid S, et al. (2022) New challenges in the use of nanomedicine in cancer therapy. *Bioengineered* 13: 759-773.
9. Su Z, Dong S, Zhao SC, Liu K, Tan Y, et al. (2021) Novel nanomedicines to overcome cancer multidrug resistance. *Drug Resistance Updates* 58: 100777.
10. Wu W, Pu Y, Shi J (2022) Nanomedicine-enabled chemotherapy-based synergetic cancer treatments. *J Nanobiotechnology* 20: 4.
11. Lopez-Goerne T, Padilla-Godinez FJ (2023) Catalytic nanomedicine as a therapeutic approach to brain tumors: Main hypotheses for mechanisms of action. *Nanomaterials* 13: 1541.
12. Gonzalez-Larraza PG, Lopez-Goerne TM, Padilla-Godinez FJ, Gonzalez-Lopez MA, Hamdan-Partida A, et al. (2020) IC50 Evaluation of platinum nanocatalysts for cancer treatment in Fibroblast, HeLa, and DU-145 Cell Lines. *ACS Omega* 5: 25381-25389.
13. Maya-Espinosa G, Collazo-Navarrete O, Millan-Aldaco D, Rivero MP, Flores GG, et al. (2015) Mouse embryonic stem cell-derived cells reveal niches that support neuronal differentiation in the adult rat brain. *Stem Cells* 33: 491-502.
14. Chang JC (2016) Cancer stem cells. *Medicine* 95: S20-S25.
15. Wei G, Wang Y, Yang G, Wang Y, Ju R (2021) Recent progress in nanomedicine for enhanced cancer chemotherapy. *Theranostics* 11: 6370-6392.
16. Lopez T, Ortiz-Islas E, Guevara P, Gomez E (2013) Catalytic nanomedicine technology: Copper complexes loaded on titania nanomaterials as cytotoxic agents of cancer cell. *Int J Nanomedicine* 8: 581-592.
17. Lopez T, Figueras F, Manjarrez J, Bustos J, Alvarez M, et al. (2010) Catalytic nanomedicine: A new field in antitumor treatment using supported platinum nanoparticles. In vitro DNA degradation and in vivo tests with C6 animal model on Wistar rats. *Eur J Med Chem* 45: 1982-1990.
18. Erdmann F, Frederiksen LE, Bonaventure A, Mader L, Hasle H, et al. (2021) Childhood cancer: Survival, treatment modalities, late effects and improvements over time. *Cancer Epidemiol* 71: 101733.
19. Lopez-Goerne TM, Padilla-Godinez FJ, Castellanos M, Perez-Davalos LA (2022) Catalytic nanomedicine: A brief review of bionanocatalysts. *Nanomedicine* 17: 1131-1156.
20. Lopez T, Sanchez E, Gomez R, Ioffe L, Borodko Y (1997) Platinum acetylacetonate effect on sol-gel derived titania catalysts. *Reaction Kinetics and Catalysis Letters* 61: 289-295.